RESEARCH DEPARTMENT

The measurement of re-radiation from lattice masts at v.h.f.

RESEARCH REPORT No. E-098

1964/30

THE BRITISH BROADCASTING CORPORATION
ENGINEERING DIVISION

RESEARCH DEPARTMENT

THE MEASUREMENT OF RE-RADIATION FROM LATTICE MASTS AT V.H.F.

Research Report No. E-098
(1964/30)

P.C.J. Hill, Ph.D., B.Sc., Grad. I.E.E.

(W. Proctor Wilson)

Report No. E-098

THE MEASUREMENT OF RE-RADIATION FROM LATTICE MASTS AT V.H.F.

May 1964 Research Report No. E-098
(1964/30)

THE MEASUREMENT OF RE-RADIATION FROM LATTICE MASTS AT V.H.F.

SUMMARY

The re-radiation coefficient of a lattice mast which is more than a small fraction of a wavelength wide cannot be calculated theoretically without making assumptions which may not be entirely valid. Re-radiation coefficients of lattice masts have therefore been measured with models, for both vertical and horizontal polarization and the full range of mast sizes likely to be encountered at v.h.f. The experimental method is described, and the results compared with re-radiation coefficients derived by approximate theoretical methods.

1. INTRODUCTION

An obstacle mast may perturb the transmission from a v.h.f. aerial mounted on an adjacent mast in a number of ways; these may be conveniently classified as follows:

(a) The mast distorts the field in the immediate vicinity of the aerial; this situation exists if the mast is itself the support structure for the aerial array, and is taken into account at the aerial design stage.

(b) The mast distorts only the radiation field of the aerial; the resultant e.r.p. in any given direction becomes frequency-dependent and may be reduced or increased.

(c) When the separation between the mast and aerial is large the re-radiated signal, which is delayed in time, may produce noticeable 'ghosting' on television transmissions.

It is the last two effects, (b) and (c), which must be taken into account if it is found necessary to erect a second mast on or very close to an existing site. It is then important to know what is the greatest amplitude of re-radiated signal likely to be encountered in the distant field, and whether there is an optimum orientation of the second mast to minimize the re-radiated field in certain directions.

If the mast is a perfectly-conducting cylinder the re-radiated field may be calculated by Carter's method;[1,2] this solution may also be applied with small error to perfectly conducting masts of square cross-section and of side width less than one half wavelength, by replacing them by an equivalent cylinder. If the mast is an open lattice structure not exceeding a very small fraction of a wavelength in width, the equivalent solid cylinder is still a good approximation. At v.h.f., however, the side width of a lattice mast may be between $0{\cdot}2\lambda$ and 2λ, where λ is the wavelength, and the theory becomes inadequate. It is therefore necessary to measure the re-radiation from lattice masts over this range; it is the purpose of this report to describe the results of such experiments.

The re-radiation coefficient $\rho(\phi)$ of a mast or other obstacle varies with the angle ϕ between the directions of the source and observer, shown in Fig. 1. Provided the distance between the source and the mast is more than ten times the width of the mast, $\rho(\phi)$ may be expressed in the form[2]

$$\rho(\phi) = F\, g(\phi)\, (d/\lambda)^{-\frac{1}{2}} \qquad (1.1)$$

where d is the distance between the source and the mast and F is the factor by which the re-radiation from the actual mast differs from that of an identical structure of infinite height.* The properties of the mast structure are most conveniently expressed in terms of the normalized re-radiation coefficient $g(\phi)$, since this quantity is independent of the height of the mast or its distance from the source.

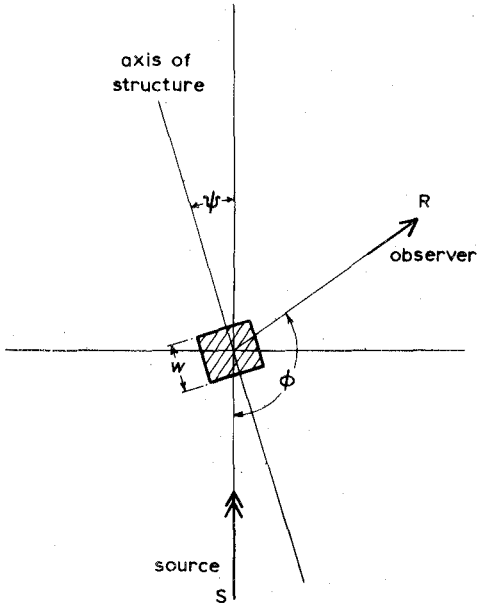

Fig. 1 - Re-radiation from an obstacle

To specify the scattering performance of a mast completely, $g(\phi)$ must be stated in terms of the width of the mast w and its orientation ψ (Fig. 1) relative to the direction of the source. The range of variables may however be reduced since, from reciprocity considerations, the re-radiation coefficient $g(\phi)$ for an orientation ψ is equal to $g(-\phi)$ for an orientation $\psi-\phi$. In addition, any symmetry in the mast cross-section reduces the range of variables still further.

In order to reduce the experimental work to a sensible limit, the measurements were restricted to square-section lattice masts with ψ having only two values, namely 0 and $\pi/4$. The mast widths were between $0{\cdot}2\lambda$ and 2λ, measurements being performed for a sufficient number of widths to enable continuous curves of $g(\phi)$ to be plotted over this range. The measurements were performed for both vertical and horizontal polarizations.

* The determination of the 'finite mast factor' F is outside the scope of this report. A curve showing how it varies with the relative height of two closely-spaced masts is contained in reference 2.

2. EXPERIMENTAL METHOD

2.1. Principles of Measurement

The horizontal radiation pattern (h.r.p.) of the source aerial was first measured by rotating the aerial on a turntable. An obstacle mast was then added and the combination rotated; from the resultant perturbations in the h.r.p. of the source aerial the re-radiation coefficient was derived.

The experimental arrangement is shown in Fig. 2 and a typical h.r.p. in Fig. 3. As the source and mast rotate the relative phase of the direct and re-radiated fields varies, causing maxima and minima to occur in the h.r.p. From the

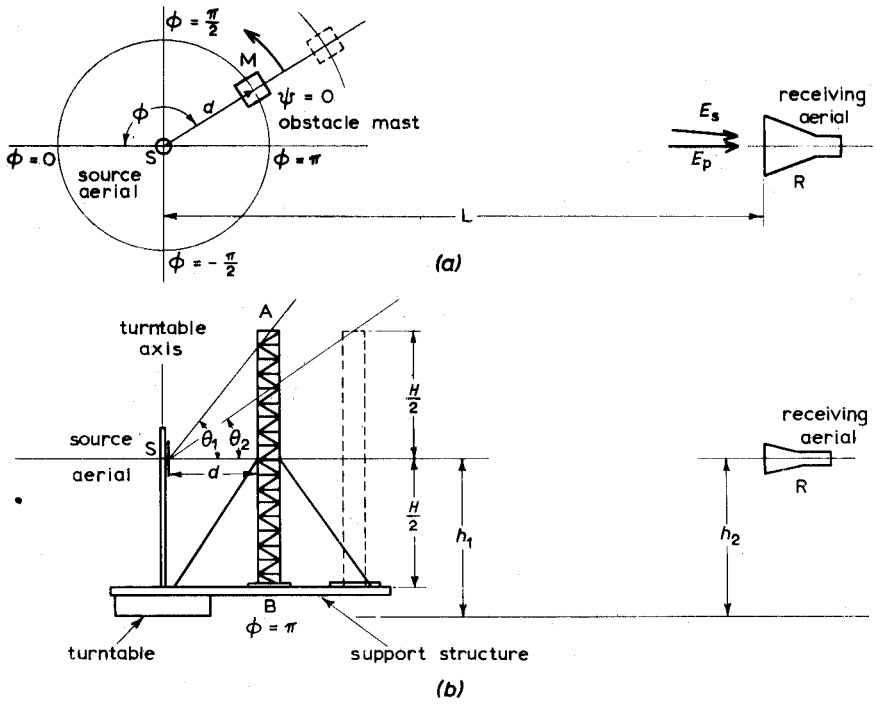

Fig. 2 - The experimental arrangement

(a) plan view (b) elevation

difference between adjacent maxima and minima it is possible to deduce the relative amplitude of the re-radiated field, and hence the re-radiation coefficient of the mast, in any particular direction. Fig. 3 shows the effect of a mast whose re-radiation coefficient varies to a considerable extent with direction.

It will be noted from Fig. 3 that the maxima or minima which occur in the directions $\phi = 0$ and π result from the symmetry of the measuring system; they must therefore be disregarded in assessing the re-radiation coefficient. The angular spacing between maxima and minima, which is greatest in these directions, must not be so large that re-radiation coefficients for these directions cannot be determined; this sets a lower limit to the distance between the source aerial and the obstacle. Although desirable, it is not essential to have an omni-directional source, because the re-radiated field depends only on the field directed at the mast, which is independent of rotation. However, the interpretation of radiation patterns of the type shown in Fig. 3 is greatly simplified if the h.r.p. of the source is approximately omni-directional.

The principal factors which determine the experimental arrangement may be summarized as follows:

(a) The spacing between source and obstacle must not be so close as to invalidate the results for more distant obstacles; this difficulty will not arise provided the spacing is at least ten times the width of the mast.

(b) The ripples in the resultant h.r.p. must be sufficiently rapid to enable $\rho(\phi)$ to be deduced accurately for all values of ϕ. This means that the spacing between source and mast must be at least 5λ.

(c) The spacing must not be so large that the re-radiated field is too small to be measured accurately. Calculation of the re-radiation coefficients of conducting cylinders of similar size indicated that the spacing should not exceed 15λ.

(d) To ensure that the measured re-radiation coefficient does not differ appreciably from that due to an infinite mast, the distances SA and SB (Fig. 2(b) must be exceeded by at least 2λ. Errors due to the finite length of the model mast may be further reduced by increasing the aperture of the source aerial; this also helps to reduce re-radiation from the support structure, particularly if the vertical radiation pattern (v.r.p.) of the source has a minimum in the direction of the support.

(e) The distance between the receiving aerial and the source should be at least ten times the source-to-obstacle distance, and the height of the receiving aerial should be such that it is at a point of maximum field strength.

(f) To increase sensitivity and eliminate stray re-radiation the receiving aerial should possess horizontal directivity, but its beamwidth must be sufficient to receive the direct and re-radiated signals with identical gains.

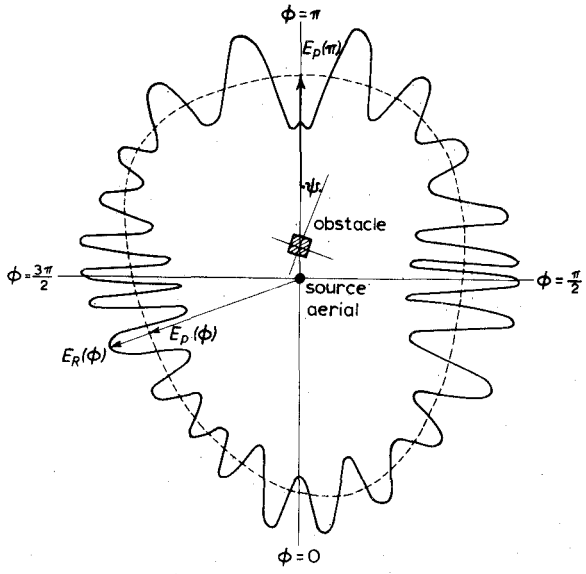

Fig. 3 - Typical h.r.p. of a source aerial in the presence of a re-radiating obstacle

------ h.r.p. of source alone
——— h.r.p. of source and obstacle

For frequencies in the range 1000 to 2000 Mc/s (wavelengths over the range 15 - 30 cms) these conditions are satisfied with a spacing between source and obstacle of 5 ft (1·5 m) for mast widths up to $1{\cdot}4\lambda$, a spacing of 9 ft (2·7 m) being adopted for wider masts. The use of a 2 : 1 range of measuring frequency enables the re-radiation coefficients of masts of any width between $0{\cdot}2$ and $2{\cdot}6\lambda$ to be measured with only four models. Moreover, the mast height may be restricted to a minimum of 10λ providing a directional source aerial

is employed; this means that the model heights need be no greater than 10 ft (3 m). In the experimental work to be described, the use of higher frequencies and smaller models was not possible, because measuring equipment tunable over a wide range of frequencies was not readily available.

2.2. Description of the Equipment

The models were based on a typical 4 ft (1·2 m) square lattice mast of the dimensions shown in Fig. 4; the sizes of the four models are given in Table 1.

TABLE 1

MODEL		MEASUREMENT	SPACING d		
No.	Width	RANGE $w(\lambda)$	ft	m	λ
1	2½ in (6·35 cm)	0·2 - 0·4λ	5	1·5	5 - 10
2	4½ in (11·4 cm)	0·375 - 0·75λ	5	1·5	5 - 10
3	8½ in (21·6 cm)	0·7 - 1·4λ	5	1·5	5 - 10
4	15½ in (39·4 cm)	1·3 - 2·6λ	9	2·7	9 - 18

Models 1 and 2 were constructed of brass to provide sufficient rigidity, and the larger models employed light alloy to minimize the bending moment on the support structure. The length of all four masts was approximately 10 ft (3 m) and they were held upright on the rotating arm by four adjustable nylon stays. The rigidity of the models was increased by including internal diagonal cross-members. The support structure was provided with a removable extension arm for use with the largest model.

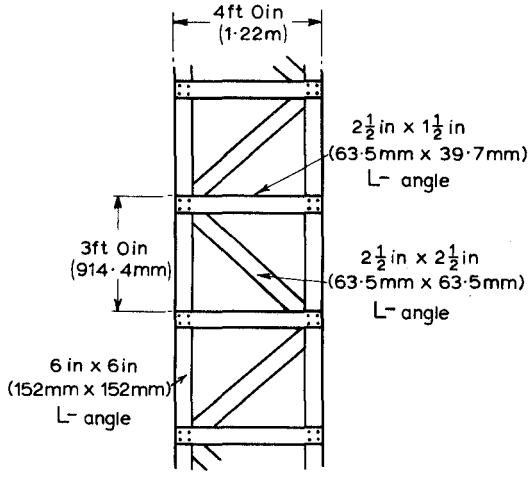

Fig. 4 - Four foot square section, lattice mast

The source aerials were carried on a 5 ft (1·5 m) Tufnol pole mounted on the turntable axis (Fig. 2(b)) and were adjusted to provide a beam of radiation towards the centre of the mast structure; down-leads were connected through Pawsey stubs located symmetrically to minimize re-radiation from the outer conductors of the cables. The sources were chosen as follows:

(a) *Vertical Polarization*

A vertical dipole on a non-metallic support pole exhibits an almost omni-directional h.r.p. The theoretical v.r.p. is given by:

$$E \propto \frac{\cos \beta h - \cos(\beta h \sin\theta)}{\cos\theta} \qquad (2.1)$$

where $2h$ is the length of the dipole, $\beta = 2\pi/\lambda$, and θ is the angle to the horizontal. The zeros of this v.r.p. are given by $\cos \beta h = \cos(\beta h \sin\theta)$ and the first null may be adjusted to fall at elevations $\theta = \pm 45°$ for $d = 5$ ft (1·5 m), and at $\theta = \pm 29°$ for $d = 9$ ft (2·7 m), by making βh equal to 3·7 or to 4·2 radians respectively at all measurement frequencies. This aerial was chosen because it required only one adjustment for each measurement frequency. The alternative arrangement of a vertically-stacked pair of half-wave dipoles requires more adjustment, and offers no additional advantages.

(b) *Horizontal Polarization*

The source chosen was the horizontal-vee or quadrant aerial[3] with an apex angle $\alpha = 90°$ and a leg length $l = \lambda/2$. Two such aerials were stacked vertically to achieve the required vertical directivity, as shown in Fig. 5; both s and l were adjustable. The array factor of the aerial is:

$$E \propto 2 \cos(\beta s \sin\theta) \qquad (2.2)$$

and has first minima occurring at elevation $\theta = \sin^{-1} \lambda/4s$. Quadrant separations $2s$ of $0{\cdot}71\lambda$ for $d = 5$ ft (1·5 m) and $1{\cdot}0\lambda$ for $d = 9$ ft (2·7 m) were therefore used.

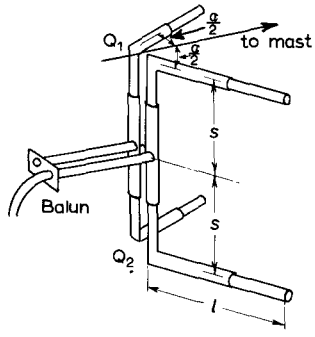

Fig. 5 - The twin quadrant aerial

The impedance of the balanced line Q_1Q_2 was designed to reduce the mismatch of the two parallel quadrants to the coaxial cable.

3. EXPERIMENTAL RESULTS

The source aerials were first checked for smoothness of h.r.p. and for vertical directivity at a few frequencies in the measurements band. Typical h.r.p.s for the two sources with the full mast support structure are shown in Fig. 6. It was

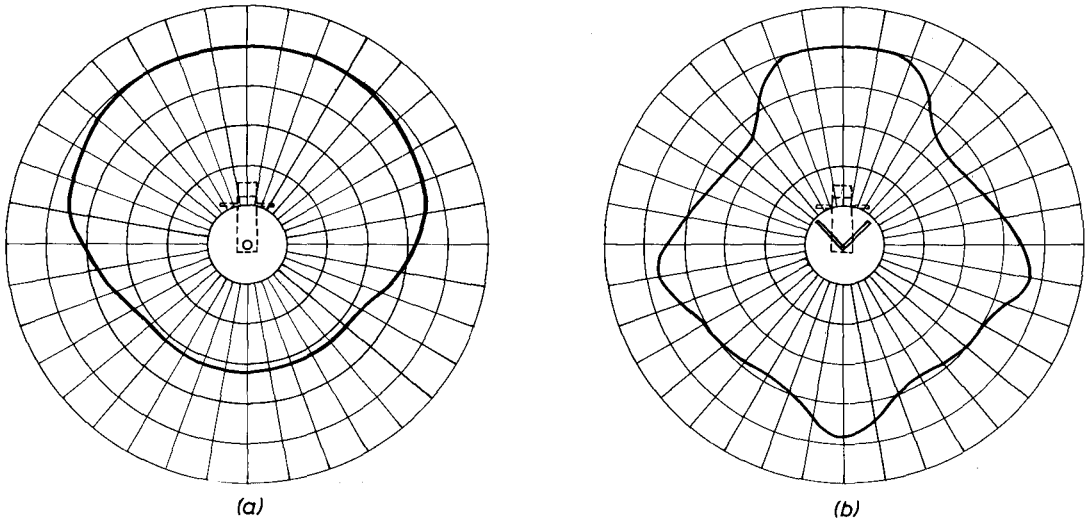

Fig. 6 - Measured h.r.p.s of source aerials at 1138 Mc/s with full mast support structure

(a) Vertically-polarized aerial (dipole) (b) Horizontally-polarized aerial (quadrant)

found that the h.r.p. of the vertical aerial was sufficiently smooth and uniform to allow it to be deduced from patterns perturbed by obstacle re-radiation. On the other hand, the h.r.p.s were less smooth with horizontal polarization, and it was

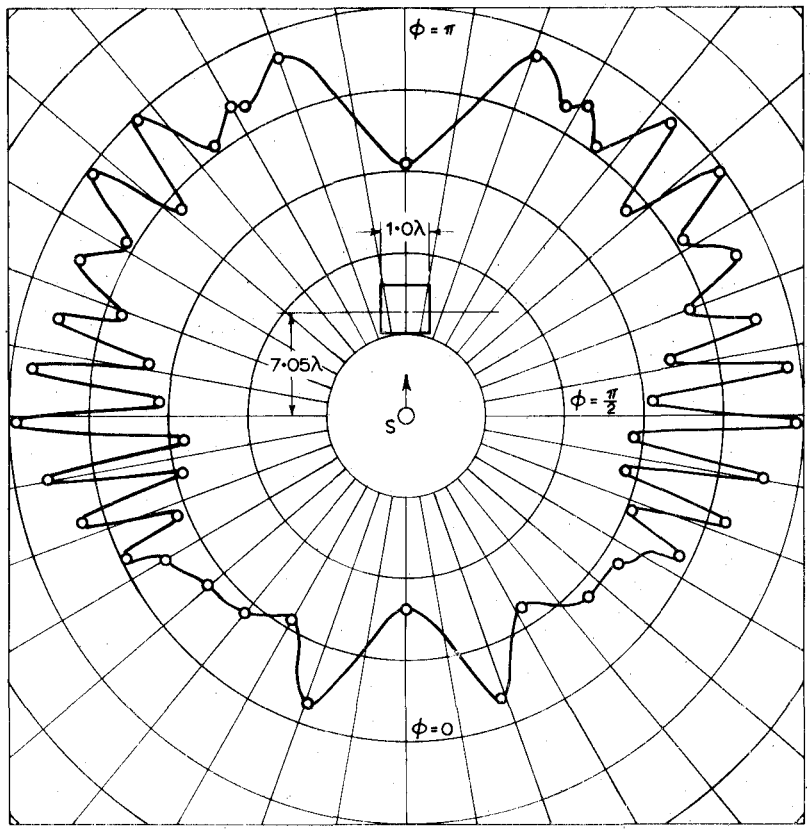

Fig. 7 - Measured h.r.p. of vertically polarized source in the presence of a lattice mast with normal incidence

S = Vertical dipole 7·4 radians long f = 1390 Mc/s

necessary to measure the source h.r.p. separately at each frequency. Typical measured h.r.p.s of a source in the presence of an obstacle are shown in Fig. 7 (vertical polarization) and in Fig. 8 (horizontal polarization).

The measured normalized re-radiation coefficient of infinite square-section lattice masts of widths up to two wavelengths were plotted as a function of mast width. Separate curves were plotted for the delayed image region of $\phi = 0$, the shadow region $\phi = \pi$, and the side region $\phi = \pi/2$ for normal and diagonal incidence of vertically and horizontally polarized waves.

3.1. Vertical Polarization

In order to check the experimental arrangement and investigate the accuracy of measurement, the re-radiation coefficients of substantially perfectly-conducting cylinders were measured and compared with theoretical values; agreement was within 5%.

Experimental results obtained from the square-section lattice masts are displayed in Figs. 9 and 10. With vertical polarization, we should expect the major contribution to the secondary field to be that re-radiated by the vertical pillars of

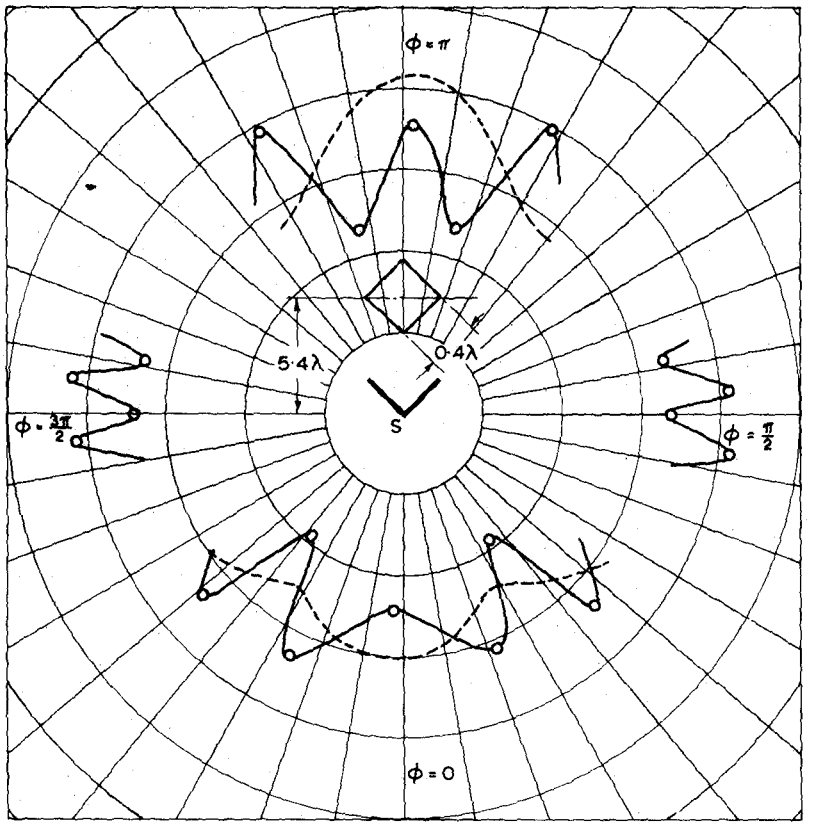

Fig. 8 - Measured h.r.p. of horizontally polarized source in the presence of a lattice mast with diagonal incidence

S = Quadrant aerial with separation 0·7λ f = 1060 Mc/s

------h.r.p. of source alone

the mast, since the currents induced in the cross-members are relatively small. For this reason, the equivalent cylinder would not be expected to give an accurate representation of the scattering performance of a lattice mast even if the width of its faces were less than 0·5λ.

The shape of the curves shown in Figs. 9 and 10 may be understood by considering the re-radiation due to the currents induced in the mast pillars. If the width of these pillars is a small fraction of a wavelength, they may be replaced by filaments situated at their current centroids. If the mutual impedance between the filaments be neglected the amplitudes of the currents may be assumed to be equal; their relative phases depend on the orientation of the mast relative to the incident radiation. If the wave is incident normally on the face of the mast, as in Fig. 11 (b), the currents in filaments A and B will be co-phased and in C and D they will lag by $2\beta a$ radians, where $2a$ is the distance between adjacent filaments. It follows that the re-radiation in the direction $\phi = \pi$ should increase steadily with the width

of the mast.* Fig. 9 shows that this is not entirely the case; the oscillations in the curve are probably due to the effects of mutual impedance. In the direction of $\phi = \pi/2$ the re-radiation would be expected to be least when the distance between the filaments is an odd number of half-wavelengths and greatest when it is a multiple of a wavelength. The measured curve (Fig. 9) is consistent with this, the positions of the maxima and minima occurring for mast widths slightly greater than the predicted values; this is because the width of the mast is a little greater than the distance between the equivalent filaments. In the direction $\phi = 0$ maxima are to be expected when the distance between the filaments is an even multiple of $\lambda/4$ and minima when

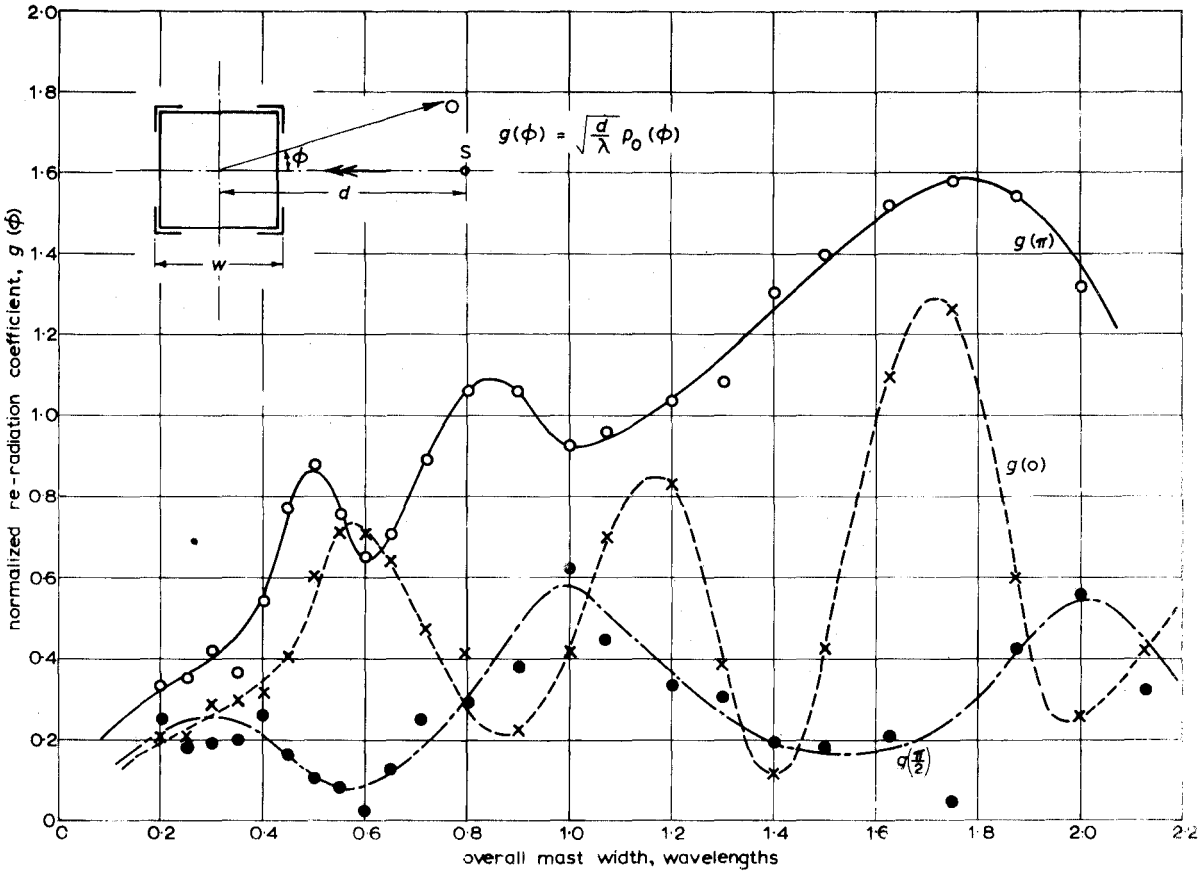

Fig. 9 - Measured normalized re-radiation coefficient of infinite lattice mast with vertical polarization and normal incidence

it is an odd multiple of $\lambda/4$; again the shape of the measured curve is consistent with this explanation. Similar considerations may be applied to the case of diagonal incidence (Fig. 11(c)); the measured results (Fig. 10) in the directions $\phi = 0$ and $\pi/2$ are again generally consistent with predictions. The large variations in the measured curve for the $\phi = \pi$ direction may be explained qualitatively on the basis that the total power scattered by the mast would be expected to increase monotonically with mast width; the fact that the maxima and minima in the $\phi = \pi$ direction do not correspond with those in the other two directions is consistent with this explanation.

* As the width of the mast increases, the size of the vertical pillars increases in proportion and the amplitude of the equivalent current filaments also increases.

A more accurate theoretical prediction of mast scattering includes the effect of the geometry of the mast pillars* and methods of taking account of this are given in the Appendix. In one method (Section 6.2.) the mast pillars are replaced

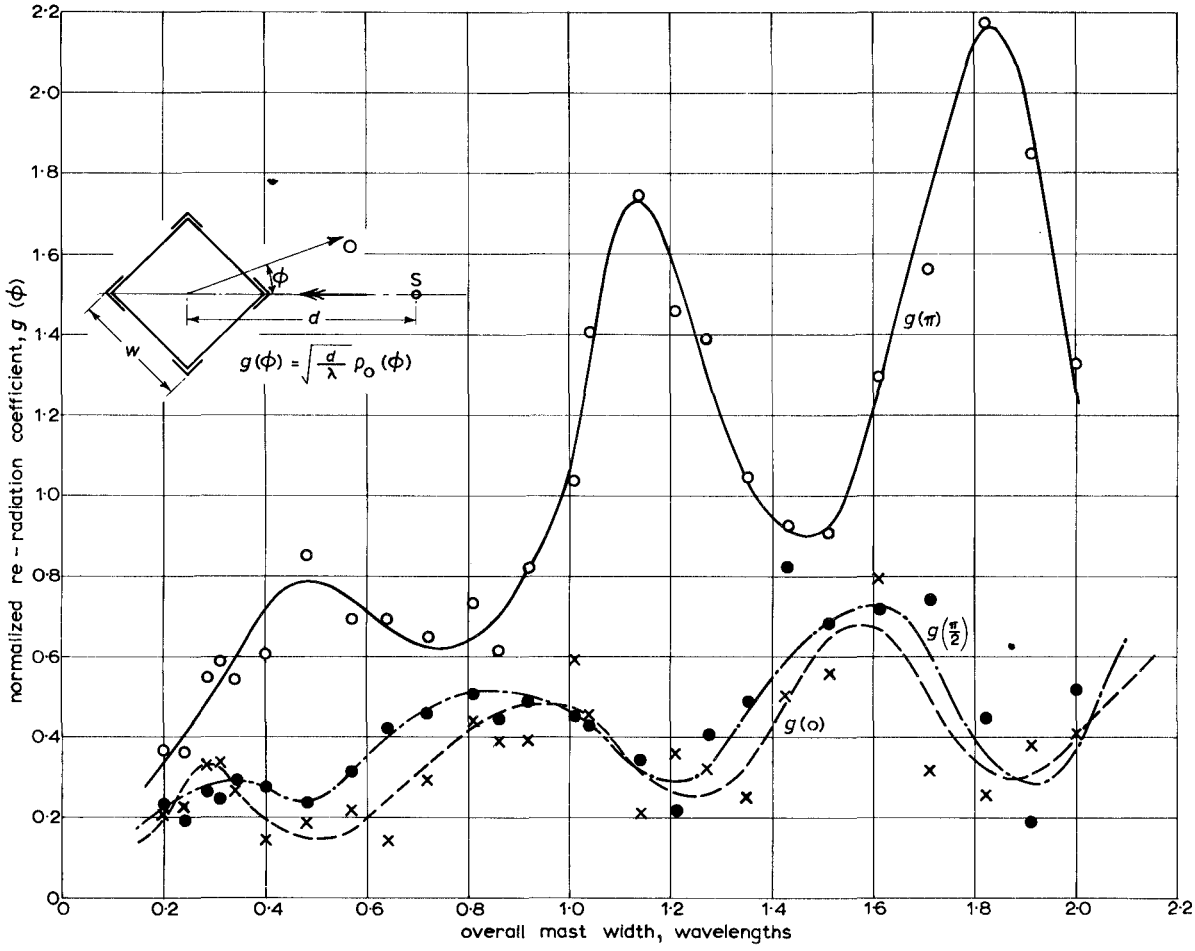

Fig. 10 - Measured normalized re-radiation coefficient of infinite lattice mast with vertical polarization and diagonal incidence

by equivalent cylinders situated at the centroids of the currents flowing in the pillars. If the mutual effects between cylinders are neglected it may be shown from superposition considerations that the normalized re-radiation coefficient of the system $g(\phi)$ is given by

$$g(\phi) = S(\phi) \cdot g_c(\phi) \tag{3.1}$$

where $g_c(\phi)$ is the normalized re-radiation coefficient of the single equivalent cylinder and $S(\phi)$ is an array factor, dependent on the orientation of the mast. In Section 6.3. of the Appendix the analysis is extended to include first-order mutual effects between the cylinders; the computed variation of re-radiation coefficient as

* Here, the mast pillars are L-shaped, as shown in Fig. 11(a).

a function of mast width for normal incidence is shown in Fig. 12 together with the

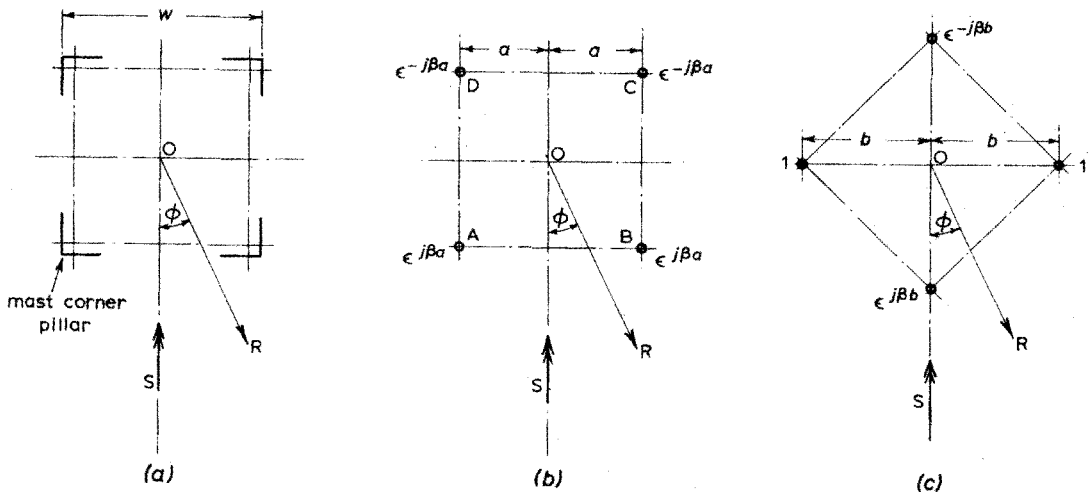

Fig. 11 - Simplified mast and equivalent structures for normal and diagonal incidence

(a) Arrangement of four mast pillars (b) Equivalent structure for normal incidence
(c) Equivalent structure for diagonal incidence

measured curves of Fig. 9. Comparison of these curves shows that the agreement is reasonably good for the range of mast sizes for which measurements were made.

3.2. Horizontal Polarization

If the primary field is horizontally polarized, the re-radiation from the mast will be mainly due to currents induced in the lattice cross-members although re-radiation from the mast pillars is still significant. Measured re-radiation coefficients for the two orientations are shown in Figs. 13 and 14.

Consideration of the re-radiation from the mast pillars of the mast alone leads to the same arguments as those which apply in the vertically polarized case, and the same maxima and minima may therefore be predicted in the measured results. With horizontal polarization, however, this effect is partly masked by the fact that loops formed by the cross members and pillars of the mast tend to resonate for certain mast sizes. Figs. 13 and 14 show that these resonances occur, with the type of structure investigated, for mast widths of approximately 0·4, 0·8 and 1·2λ; with other types of mast structure, resonances would not necessarily occur with these particular widths but would probably occur elsewhere. Despite this masking, however, the measured curves of Figs. 13 and 14 show that most of the minima due to the mast pillars are present. An analysis of mast scattering with horizontal polarization is difficult, and has not been attempted because of the number of effective re-radiating surfaces involved; the result, moreover, would apply only to a particular type of mast structure.

3.3. Interpretation of Results

As previously stated, it was not practicable to measure the scattering from lattice masts for a large number of orientations and measurements have been confined to cases in which $\psi = 0$ and $\psi = \pi/4$. For the square section mast, the results thus

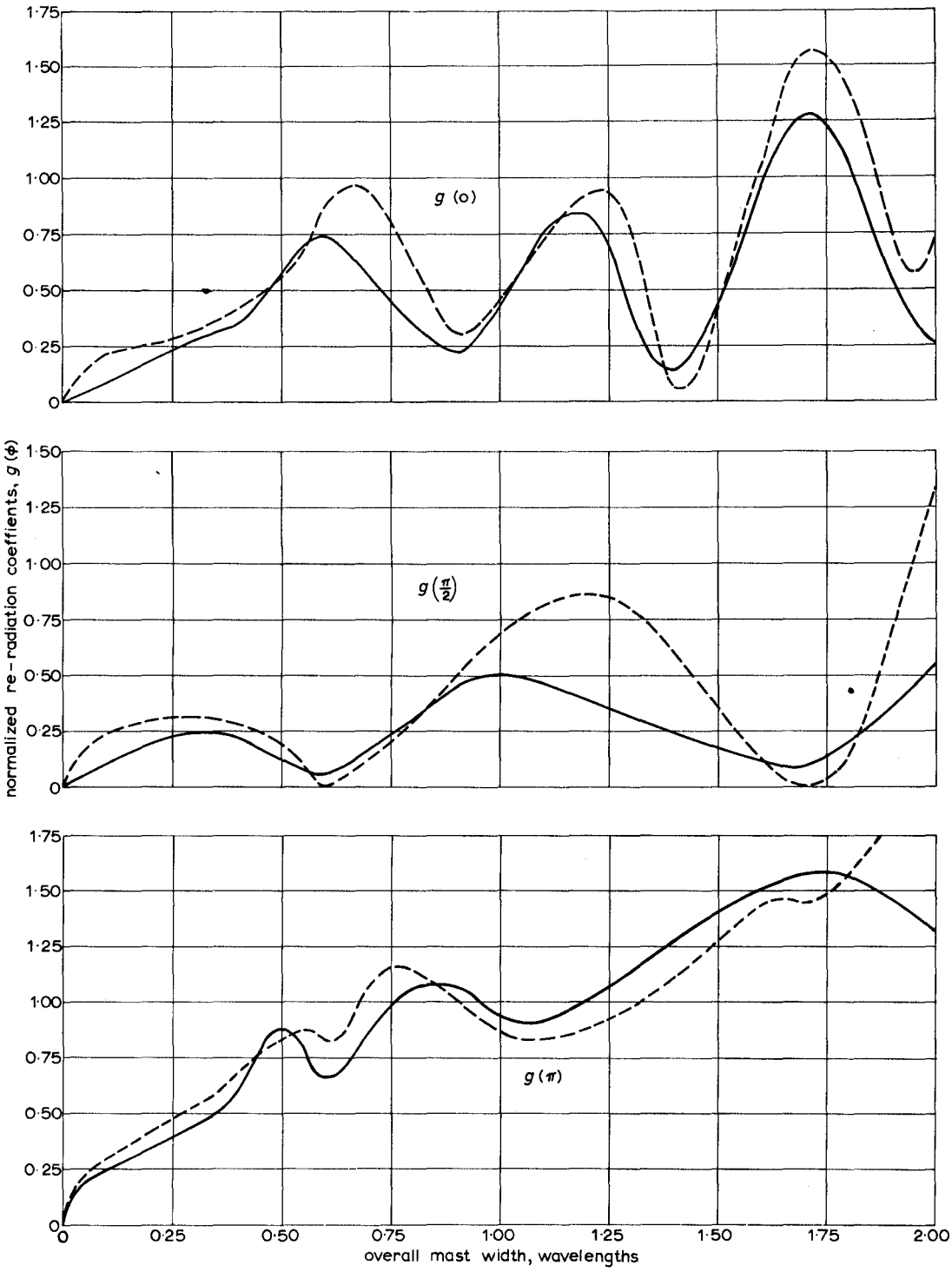

Fig. 12 - Theoretical and measured re-radiation coefficients of an infinite square section lattice mast for normal incidence with vertical polarization

---- Theoretical ——— Measured

obtained apply to a total of eight symmetrically related orientations. In a practical case, however, it may be necessary to estimate the re-radiation coefficient of a mast at some arbitrary orientation to the incident field. In order to satisfy this requirement the curves showing the variation of re-radiation coefficient with mast

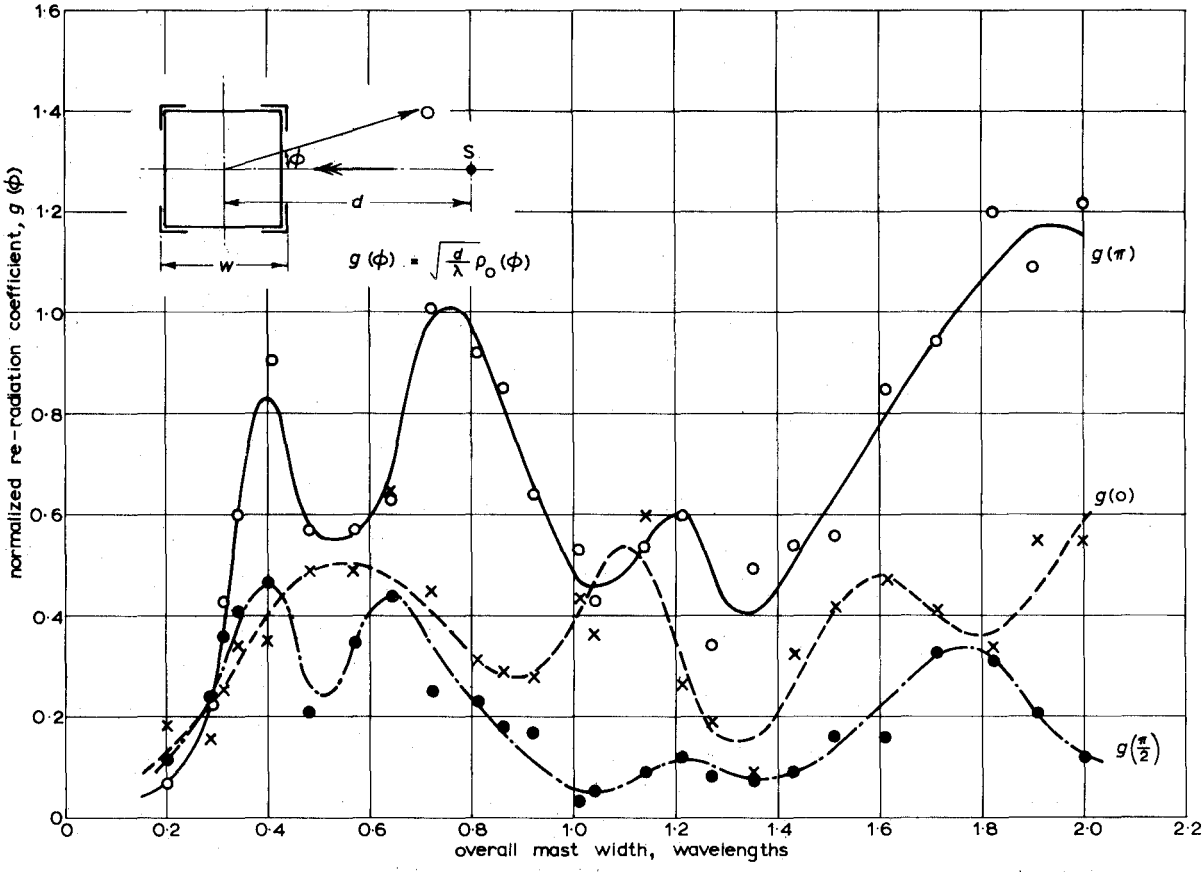

Fig. 13 - Measured normalized re-radiation coefficient of infinite lattice mast with horizontal polarization and normal incidence

width for vertical polarization (Figs. 9 and 10) and those for horizontal polarization (Figs. 13 and 14) have been compressed into the practical curves of Figs. 15 and 16 respectively. These smoothed curves show probable upper limits for the re-radiation coefficients of infinite square section lattice masts of arbitrary orientation for the three directions $\phi = 0$, $\pi/2$ and π.

The smoothed results of Figs. 15 and 16 were derived by superposing the appropriate curves for normal and diagonal incidence and drawing their envelope. This procedure may be justified by the fact that the principal effect of changing the mast orientation with a fixed source and observer is to vary the relative phase of the re-radiation from individual structural members of the mast; this causes the maxima and minima of the curves to occur at different mast sizes without greatly affecting the amplitudes of the maxima.

For comparison purposes, curves showing theoretical re-radiation coefficients for the equivalent cylinder* are also shown in Figs. 15 and 16 although there is no

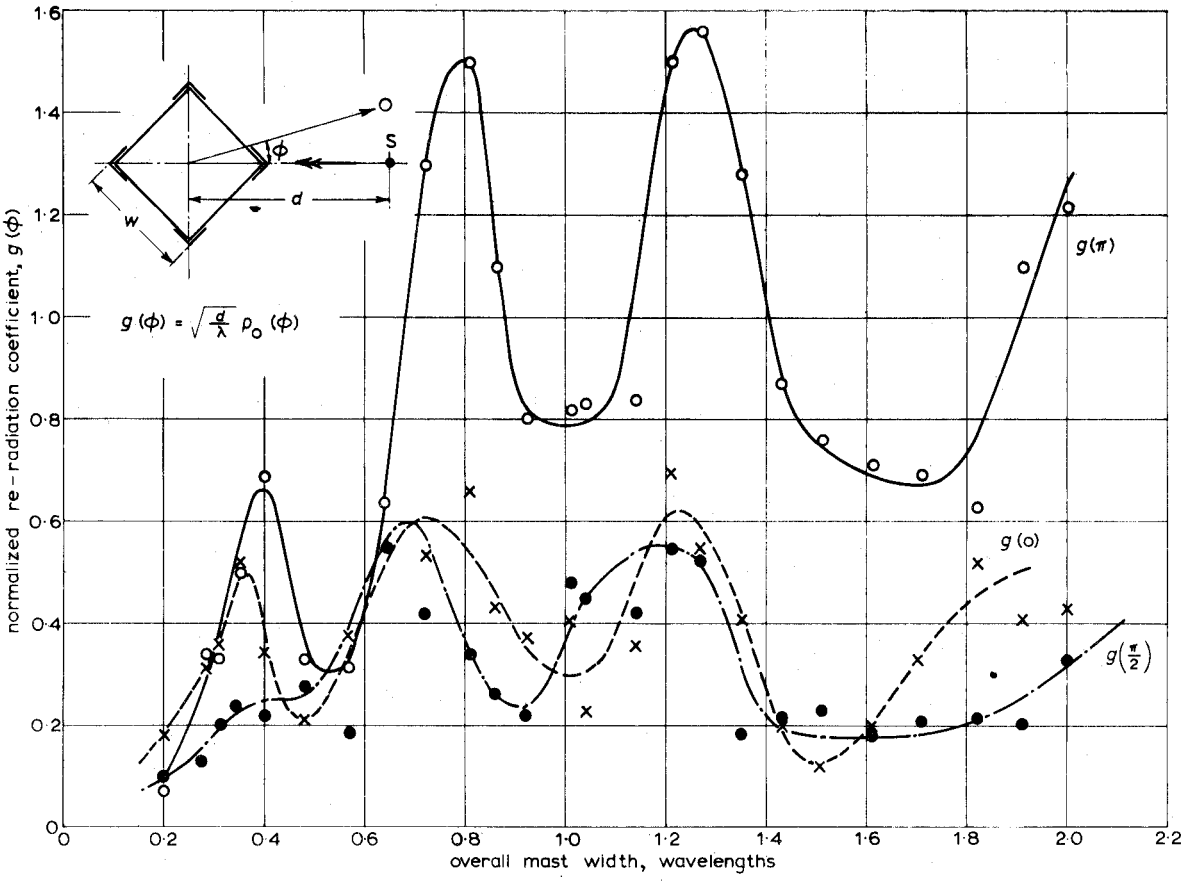

Fig. 14 - Measured normalized re-radiation coefficient of infinite lattice mast with horizontal polarization and diagonal incidence

theoretical justification for the use of an equivalent cylinder in this case. In fact the agreement between the cylinder curves and the smoothed curves is reasonably good.

4. CONCLUSIONS

The measurements described in this report show that the re-radiation coefficient of a lattice mast of given size can vary over a considerable range, the actual value depending on the polarization of the incident wave, on the orientation of the mast relative to the incident wave and on the direction of the observer. Although not confirmed experimentally, the re-radiation coefficient is believed to depend to some extent upon the type of lattice structure employed.

* The radius of the equivalent cylinder is 0·59 times the width of the mast face; a cylinder of this radius has the same capacitance per unit length as a non-lattice square-section conductor provided the width of the conductor is small compared with the wavelength. In practice the capacitance of the equivalent cylinder is a reasonably good approximation to that of a square-section conductor for widths up to 0·5λ.

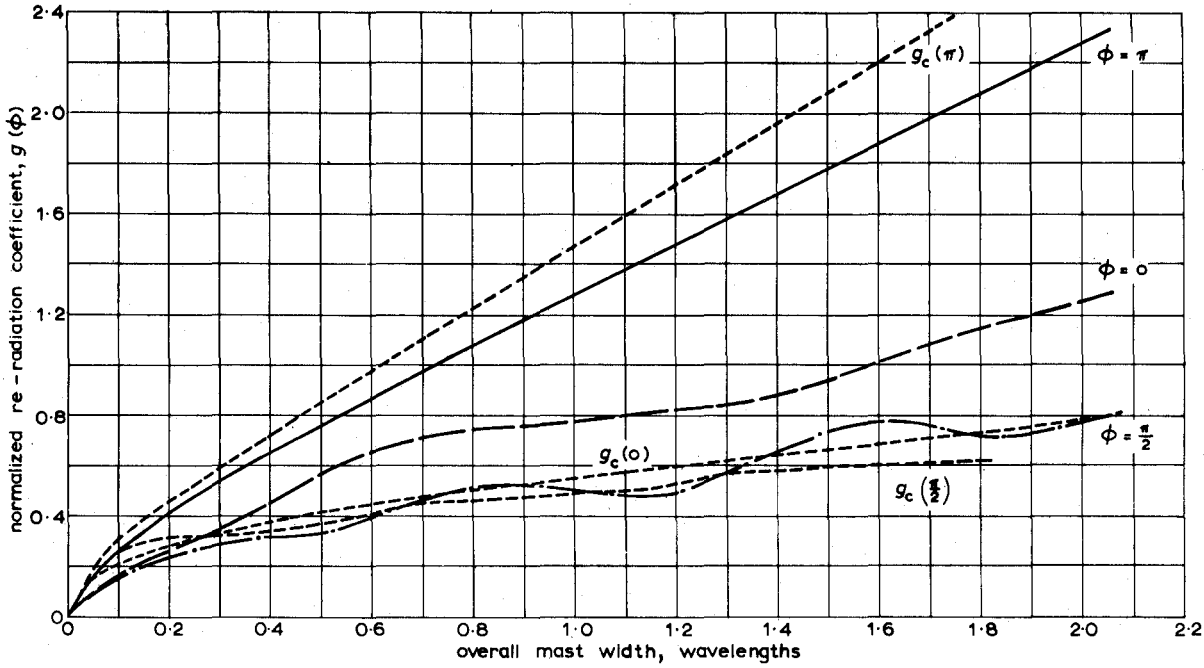

Fig. 15 - Re-radiation coefficient of infinite square section lattice mast - probable upper limit for arbitrary orientation with vertical polarization

——— Curves deduced from measurements
– – – – – Equivalent cylinder curves, $g_c(\phi)$

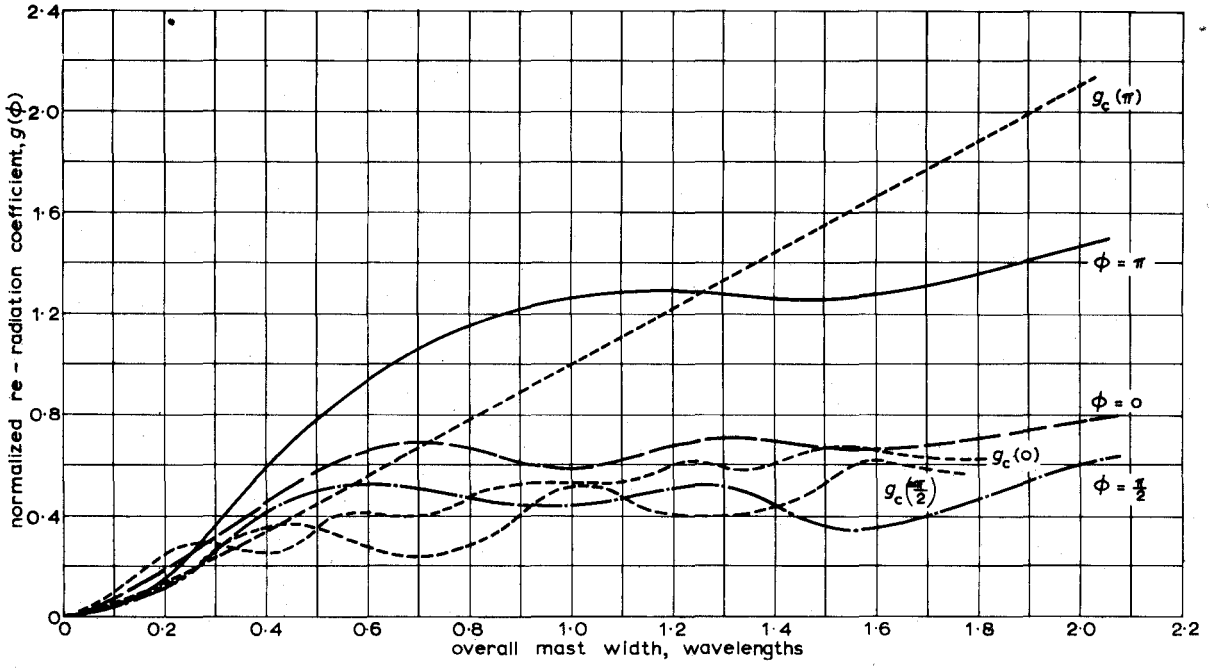

Fig. 16 - Re-radiation coefficient of infinite square section lattice mast - probable upper limit for arbitrary orientation with horizontal polarization

——— Curves deduced from measurements
– – – – – Equivalent cylinder curves, $g_c(\phi)$

In view of these large variations the detailed results contained in this report should be restricted to the particular cases investigated. Upper limits for the re-radiation coefficients for other orientations and for other types of square-section masts may, however, be derived from Figs. 15 and 16. These curves may also be used as a guide in estimating the re-radiation coefficients of masts of other shapes. For example the maximum re-radiation of a triangular mast of width w would be expected to be the same as that of a square mast of width $w/\sqrt{2}$, since both masts have the same maximum projected area.

Although an explanation of the shape of the re-radiation coefficient curves for lattice masts can be given on a qualitative basis, a detailed theoretical treatment presents considerable difficulties, particularly in the case of horizontal polarization. With vertical polarization the major contribution to re-radiation is from the vertical pillars of the mast and a good theoretical estimate of re-radiation coefficient may be produced by analysing a system of four thin equivalent cylinders placed at the corners of a square; this analysis has been found reasonably accurate for square masts up to one wavelength wide. No satisfactory theoretical method has been evolved for the case of horizontal polarization.

Prior to this investigation, lattice masts were assumed to be equivalent to solid conductors of the same size and shape; these in turn were assumed to be equivalent to cylindrical conductors. The re-radiation coefficient for the cylinder was then calculated by an exact theoretical method.

Although there is little theoretical justification for applying this method to masts more than $0{\cdot}5\lambda$ wide, the measurements described in this report have shown that this method gives a reasonably accurate indication of the maximum value of re-radiation coefficient which is likely to occur with square-section lattice masts up to two wavelengths in width.

5. REFERENCES

1. Carter, P.S.: 'Antenna Arrays around Cylinders', *Proc. I.R.E.*, 1943, (**31**, 12, p.671).

2. 'Reflexions from Masts at Very High Frequencies', Research Department Technical Memorandum No. E-1065, December 1961.

3. Wells, N.: 'An Omni-Directional Wideband Horizontal Aerial for Short Waves', *Proc. I.E.E.*, March 1944, (**91 III**, 13, p.182).

4. See for example: Jordan, E.C.: 'Electromagnetic Waves and Radiating Systems', (Prentice-Hall Inc., New York, 1950) pp.598-605.

6. APPENDIX *The Re-radiation Coefficient of Four Vertical Infinite Cylinders Placed on the Corners of a Square*

6.1. Introduction

Three methods are described for determining the re-radiation coefficient of a set of four parallel infinite cylinders placed at the corners of a square. The analysis is restricted to the special case of vertically polarized waves incident normally to the cylinder set as shown in Fig. 17; the methods of solution adopted here may however be extended to systems with horizontal polarization and arbitrary wave incidence.

The first method of solution ignores all mutual effects between the cylinders; the second method includes mutual effects but assumes that the cylinder radii are small; the third method combines the two previous solutions and applies to a system in which the cylinder size is not necessarily small compared with the spacing. The nature of the problem is first outlined.

The problem of re-radiation from a single cylinder is well-known[4] but is included here for the sake of completeness.

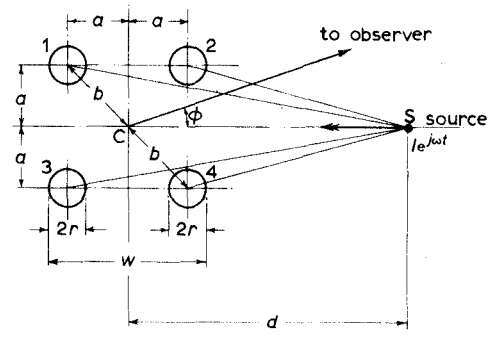

Fig. 17 - Plan view of four vertical cylinders placed on the corners of a square, scattering vertically polarized waves incident from a source positioned normal to the side of the square

Referring to Fig. 18, the vector potential* **A** at a point P distant ρ' from

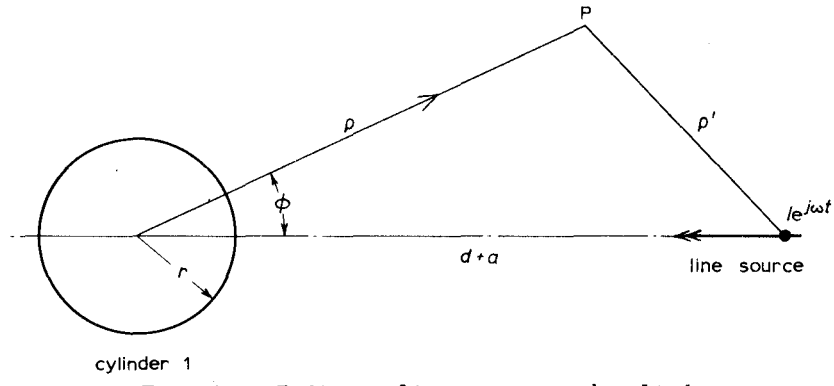

Fig. 18 - Infinite line source and cylinder

an infinite line current source carrying a current $Ie^{j\omega t}$ may be written:

$$A_z = kH_0^{(2)}(\beta\rho') \tag{6.1}$$

where $k = -j\mu_0 I/4$ and $H_0^{(2)}$ denotes the Hankel function of the second kind of zero order. In deriving equation (6.1) the z-axis was assumed to coincide with the line source and the time factor $e^{j\omega t}$ was suppressed.

* The vector potential **A** is defined by the relation **B** = curl **A** where **B** is the magnetic flux density.

Using the addition theorem for Bessel functions we have for $\rho < d+a$ and $d >> a$,

$$A_{z_1} = k \sum_0^\infty \epsilon_n H_n^{(2)} (\beta \overline{d+a}) J_n(\beta\rho) \cos n\phi \tag{6.2}$$

where ϵ_n is Neumann's number ($\epsilon_n = 1$ for $n = 0$ and 2 for $n \neq 0$).

The solution may now be extended to groups of cylinders as shown in Fig. 17, equation (6.2) being used to express the waves from the source in terms of cylindrical waves originating from the front and back cylinder axes. Secondary waves from the cylinders may be written:

$$A_{z_2} = k \sum_0^\infty \epsilon_n \begin{Bmatrix} P_n \\ Q_n \end{Bmatrix} H_n^{(2)} (\beta\rho) \cos n\phi \tag{6.3}$$

where P_n, Q_n are arbitrary constants to be determined from boundary conditions and from symmetry considerations, P_n being used for cylinders 1 and 3 and Q_n for cylinders 2 and 4. Since $E_z = j\omega A_z$, the boundary conditions for each cylinder, assumed to be perfectly conducting, become:

$$A_{z_1} + \sum A_{z_2} = 0 \tag{6.4}$$

For example, for cylinder 1, equation (6.4) is written in the form,

$$\sum_0^\infty \epsilon_n H_n^{(2)} (\beta\overline{d+a}) J_n(\beta r) \cos n\phi + \sum_0^\infty \epsilon_n P_n H_n^{(2)} (\beta r) \cos n\phi + \sum S_1 + \sum S_2 + \sum S_3 = 0$$

where r is the cylinder radius and the last three terms represent the secondary fields of cylinders 2, 3 and 4 referred to the axis of cylinder 1. In general it is found impossible to solve such boundary conditions unless certain approximations are made in expressing all the secondary fields appearing in equation (6.4) in compatible form.

6.2. Solution Ignoring Mutual Effects between Cylinders

If the mutual effects between the cylinders are ignored then superposition may be applied to the problem; that is, the contribution from any one cylinder to the total re-radiation is the same as if all the other cylinders had been removed; the total secondary field is then given by the vector sum of the individual fields.

Since we are interested in the *distant* re-radiation field from a system subject to *plane wave* incidence, i.e. $\beta\rho$ large and $d \gg a$, the individual re-radiation from each cylinder may be taken as the field it would re-radiate if it were situated at the centre of the system (at C in Fig. 17) multiplied by the corresponding phase factor. The phase factors contain two terms, one due to the induced current phase at the actual cylinder axes relative to C, the other a space factor dependent on the position of the cylinders relative to the system centre and the orientation ϕ of the system with respect to the observer.

The boundary condition for a cylinder of radius r placed at the centre C is given by (6.4) which, on inserting (6.2) and (6.3) with $a = 0$, becomes:

$$\sum_{0}^{\infty} \epsilon_n H_n^{(2)}(\beta d)\, J_n(\beta r)\, \cos n\phi = - \sum_{0}^{\infty} \epsilon_n P_n H_n^{(2)}(\beta r)\, \cos n\phi$$

$$\text{i.e. } P_n = - H_n^{(2)}(\beta d)\, J_n(\beta r)/H_n^{(2)}(\beta r) \tag{6.5}$$

Substituting (6.5) into (6.3) the secondary field becomes:

$$A_{z_2} = - k \sum_{0}^{\infty} \epsilon_n \frac{H_n^{(2)}(\beta d)\, J_n(\beta r) H_n^{(2)}(\beta \rho)}{H_n^{(2)}(\beta r)} \cos n\phi \tag{6.6}$$

and for large arguments $\beta\rho$ and βd, $H_n^{(2)}(\beta\rho)$ and $H_n^{(2)}(\beta d)$ may be replaced by their asymptotic values, which simplifies (6.6) to:

$$A_{z_2} = -j \frac{k\lambda e^{-j\beta(\rho+d)}}{\pi^2\sqrt{\rho d}} \sum_{0}^{\infty} \epsilon_n (-1)^n \frac{J_n(\beta r)}{H_n^{(2)}(\beta r)} \cos n\phi \tag{6.7}$$

The normalized re-radiation coefficient of the cylinder $g_c(\phi) = \sqrt{d/\lambda}\, \rho_c(\phi)$ is given by:

$$g_c(\phi) = \sqrt{d/\lambda} \left| A_{z_2}/A_{z_1} \right| \tag{6.8}$$

since $E_z = -j\omega A_z$.

Now, the amplitude of the direct field from the source $|A_{z_1}|$ may be obtained from (6.1) since for ρ large, $\rho' \simeq \rho$ and using the asymptotic form of the Hankel function we have:

$$|A_{z_1}| = k/\pi \sqrt{\rho/\lambda} \tag{6.9}$$

Substituting (6.7) and (6.9) into (6.8), the normalized re-radiation coefficient is given by:

$$g_c(\phi) = \frac{1}{\pi} \left| \sum_{0}^{\infty} \epsilon_n (-1)^n \frac{J_n(\beta r)}{H_n^{(2)}(\beta r)} \cos n\phi \right| \tag{6.10}$$

Expression (6.10) for the normalized re-radiation coefficient of an infinite vertical cylinder to vertically polarized waves has been plotted in Fig. 2 of reference 2 for $\phi = 0$, $\pi/2$ and π.

Now, the normalized re-radiation coefficient of the system shown in Fig. 17 becomes:

$$g(\phi) = g_c(\phi) \left\{ \Phi(1) + \Phi(2) + \Phi(3) + \Phi(4) \right\} \tag{6.11}$$

where $\Phi(m)$ represents the phase factor of cylinder m, and $g_e(\phi)$ is given by (6.10) above. For normal incidence, the phase factors are

$$\begin{aligned}\Phi(1) &= e^{-j\beta a}.e^{-j\beta b\cos(\pi/4+\phi)}\\ \Phi(2) &= e^{j\beta a}.e^{j\beta b\cos(\pi/4-\phi)}\\ \Phi(3) &= e^{-j\beta a}.e^{-j\beta b\cos(\pi/4-\phi)}\\ \Phi(4) &= e^{j\beta a}.e^{j\beta b\cos(\pi/4+\phi)}\end{aligned} \tag{6.12}$$

where $b = a\sqrt{2}$

Substituting (6.12) into (6.11) and performing the summation we have:

$$g(\phi) = 4\cos(\beta a\sin\phi)\ \cos(2\beta a\cos^2\phi/2).g_e(\phi) \tag{6.13}$$

Equation (6.13) may be written as:

$$g(\phi) = S_N(\phi)g_e(\phi) \tag{6.14}$$

where $S_N(\phi)$ is the resultant space or 'array' factor for the group of cylinders subjected to normal wave incidence.

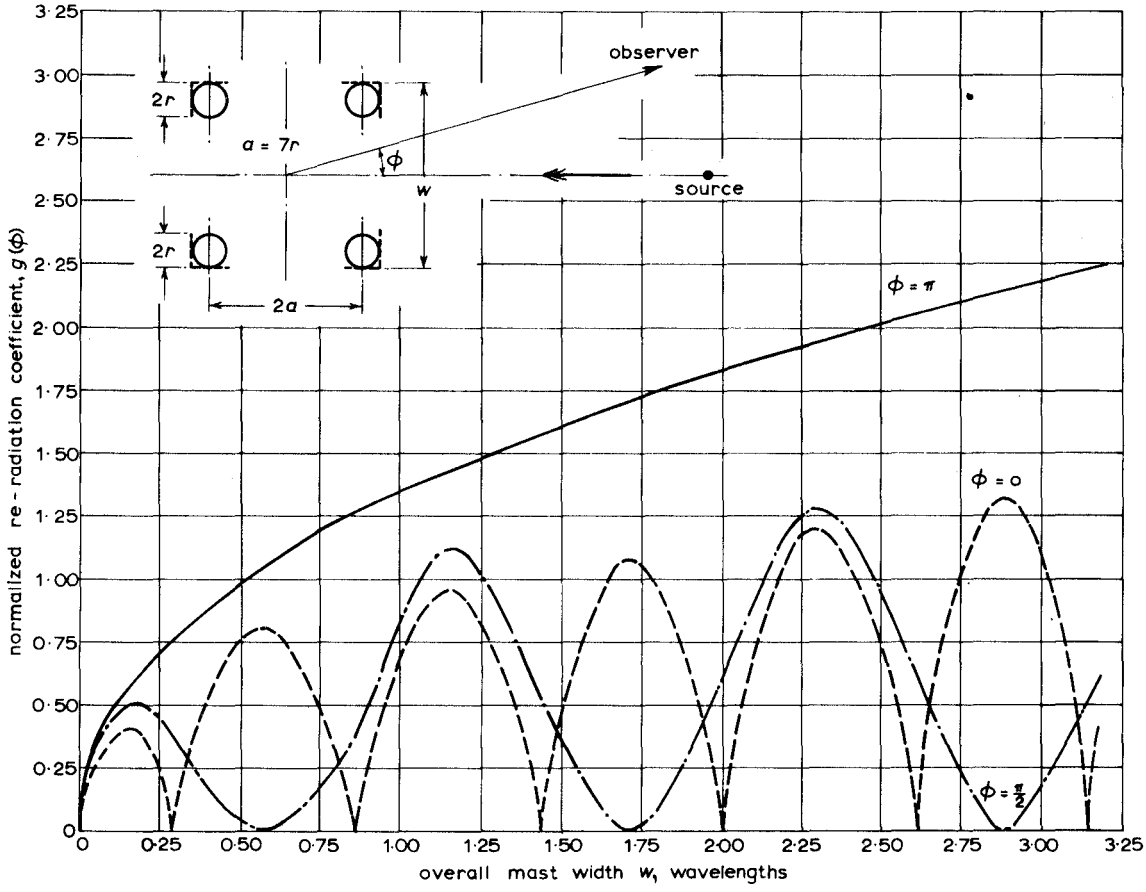

Fig. 19 - Re-radiation from four vertical infinite cylinders with vertical polarization neglecting mutual effects

From (6.13) we have:

$$g(0) = 4\cos 2\beta a.g_c(0)$$
$$g(\pi/2) = 4\cos^2\beta a.g_c(\pi/2) \qquad (6.15)$$
$$g(\pi) = 4g_c(\pi)$$

These coefficients are plotted in Fig. 19 against overall mast width w for $a = 7r$, a ratio chosen because it applies to the type of 4 ft (1·2 m) square section lattice mast for which the measurements were performed (assuming that the diameter of the cylinders is equal to the width of the mast pillars). If the curves of Fig. 19 are compared with the corresponding curves of Fig. 9 it will be seen that $g(0)$ and $g(\pi/2)$ exhibit maxima and minima at nearly identical mast widths in both cases. This is because the scattering performance of the actual lattice mast is very largely controlled by the space factor of the mast pillars, as explained qualitatively in Section 3.1, and this space factor is the same as that given by equation (6.13).

6.3. Solution including the Effect of Mutual Impedance between Thin Cylinders

If the diameters of the cylinders are very small they will re-radiate uniformly in all directions. Their re-radiation fields and reflexion coefficients

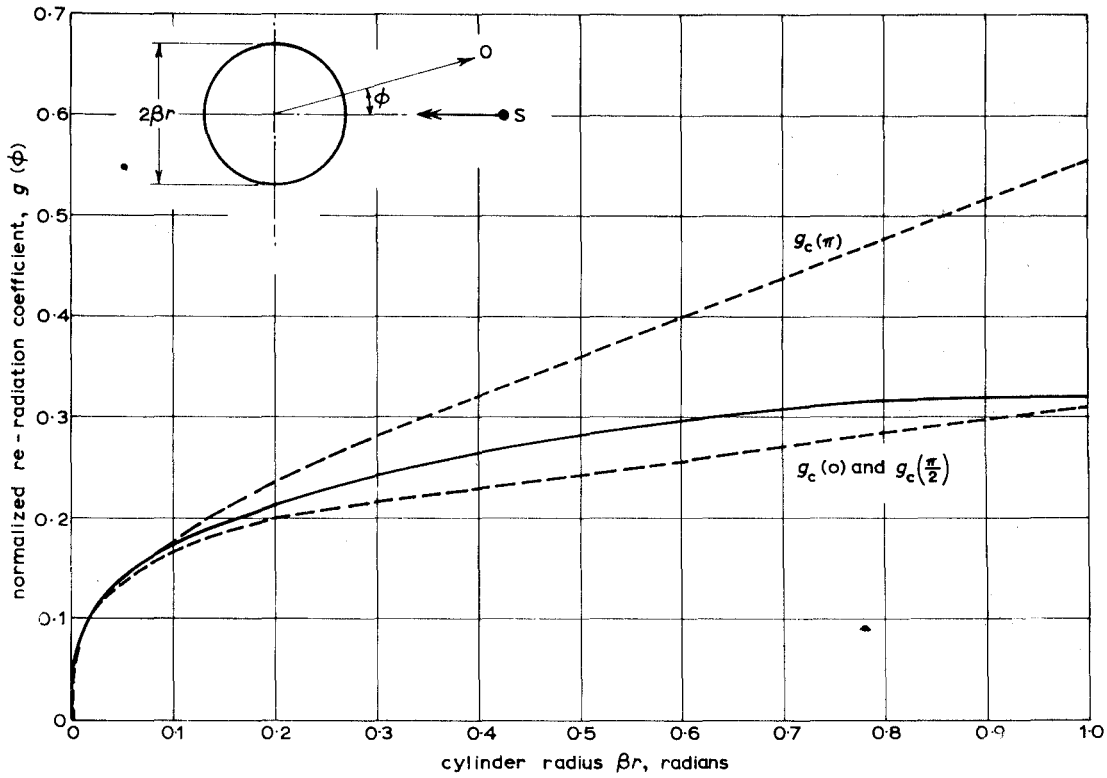

Fig. 20 - Normalized re-radiation coefficient of a thin cylinder with vertical polarization

——— Values calculated from approximate formula
– – – – – Values calculated from exact formula

may then be described by single terms, corresponding to $n = 0$ in equations (6.3) and (6.10); thus the normalized re-radiation coefficient, from equation (6.10) is given by:

$$g(\phi) = \frac{1}{\pi}\left|\frac{J_0(\beta r)}{H_0^{(2)}(\beta r)}\right| \tag{6.16}$$

The function (6.16) is plotted in Fig. 20 together with the exact values of $g_e(0)$, $g_e(\pi/2)$, and $g_e(\pi)$ given by equation (6.10). It will be observed that the solution for the thin cylinder is approximately 10% in error at a cylinder radius βr equal to 0·2 rds (0·032λ); thus if the width of a mast is eight times the width of its vertical pillars and if the latter are represented by equivalent cylinders as in Section 6.2, then the thin cylinder approximation should give reasonably accurate results for mast widths up to 0·5λ.

For the system shown in Fig. 17, it may be shown that the boundary conditions are given by the matrix relationship

$$\begin{bmatrix} H_0^{(2)}(\beta r) + H_0^{(2)}(2\beta a), & H_0^{(2)}(2\beta a) + H_0^{(2)}(2\beta b) \\ H_0^{(2)}(2\beta a) + H_0^{(2)}(2\beta b), & H_0^{(2)}(\beta r) + H_0^{(2)}(2\beta a) \end{bmatrix} \begin{bmatrix} P_0 \\ Q_0 \end{bmatrix} = \begin{bmatrix} H_0^{(2)}(\beta\overline{d+a}) \\ H_0^{(2)}(\beta\overline{d-a}) \end{bmatrix} \tag{6.17}$$

and equation (6.17) yields P_0 and Q_0. When the distance to the observer ρ_0 is large compared with the distance d between source and mast, the direct and secondary vector potentials are respectively:

$$\left|A_{z_1}\right| = k/\pi\sqrt{\rho_0/\lambda} \tag{6.18}$$

and

$$\left|A_{z_2}\right| = \frac{k}{\pi\sqrt{\rho_0/\lambda}}\left|\overline{\Phi'(1) + \Phi'(3)}\,P_0 + \overline{\Phi'(2) + \Phi'(4)}\,Q_0\right| \tag{6.19}$$

in which $\Phi'(n)$'s are the phase factors of (6.12) with the induced current phase terms $e^{\pm j\beta a}$ removed, since the latter are now included in P_0 and Q_0. Inserting these factors in (6.19) and recalling that $\rho(\phi) = \left|A_{z_2}/A_{z_1}\right|$ we have from (6.18) and (6.19):

$$\rho(\phi) = 2\cos(\beta a\sin\phi)\left|P_0 e^{-j\beta a\cos\phi} + Q_0 e^{j\beta a\cos\phi}\right| \tag{6.20}$$

from (6.17) the asymptotic values of P_0 and Q_0 are given by:

$$P_0 = \frac{e^{-j\beta a}\{H(A) + H(R)\} - e^{j\beta a}\{H(A) + H(B)\}}{\pi\sqrt{d/\lambda}\{H(R) + 2H(A) + H(B)\}\{H(R) - H(B)\}}\; e^{j(\pi/4 - \beta d)}$$

and

$$Q_0 = \frac{e^{j\beta a}\{H(A) + H(R)\} - e^{-j\beta a}\{H(A) + H(B)\}}{\pi\sqrt{d/\lambda}\{H(R) + 2H(A) + H(B)\}\{H(R) - H(B)\}}\; e^{j(\pi/4 - \beta d)} \quad \text{for } d \gg a$$

where $H(A)$, $H(B)$, and $H(R)$ are defined by:

$$H(A) = H_0^{(2)}(2\beta a)$$
$$H(B) = H_0^{(2)}(2\beta b) \qquad (6.21)$$
$$H(R) = H_0^{(2)}(\beta r)$$

On substitution into (6.20) and rationalizing we obtain:

$$\rho(\phi) = \frac{4\cos(\beta a \sin\phi)}{\pi\sqrt{d/\lambda}} \left| \frac{\{H(R)+H(A)\}\cos(2\beta a\cos^2\phi/2) - \{H(A)+H(B)\}\cos(2\beta a\sin^2\phi/2)}{\{H(R)+2H(A)+H(B)\}\{H(R)-H(B)\}} \right| \qquad (6.22)$$

Hence:
$$g(0) = \frac{4}{\pi}\left| \frac{\{H(R)+H(A)\}\cos 2\beta a - \{H(A)+H(B)\}}{\{H(R)+2H(A)+H(B)\}\{H(R)-H(B)\}} \right| \qquad (6.23)$$

$$g(\pi/2) = \frac{4\cos^2\beta a}{\pi}\left| \frac{1}{\{H(R)+2H(A)+H(B)\}} \right| \qquad (6.24)$$

$$g(\pi) = \frac{4}{\pi}\left| \frac{\{H(R)+H(A)\} - \cos 2\beta a\{H(A)+H(B)\}}{\{H(R)+2H(A)+H(B)\}\{H(R)-H(B)\}} \right| \qquad (6.25)$$

These functions (6.23), (6.24), and (6.25) have been plotted in Fig. 12 against an overall square width $w = 2(a+r)$ with $a = 7r$ as in Section 6.2. It has been shown (Fig. 20) that the thin cylinder approximation becomes inaccurate for βr greater than 0·2 radians (0·032λ) and therefore we should not expect these solutions to be accurate for masts wider than 3·2 radians (0·5λ). In fact if these solutions are compared with the measured results for the lattice mast (Fig. 12) it is seen that there is very good agreement for mast widths up to one wavelength. For mast sizes between one and two wavelengths solutions (6.23) and (6.25) remain reasonably accurate whereas (6.24) presents appreciable error..

6.4. Approximate Solution for Large Diameter Cylinders

For the sake of completeness, one method of solving the problem more accurately will be indicated. In this method the boundary conditions at each cylinder are satisfied by including all values of n to describe the self-re-radiation from the cylinder in question and only $n = 0$ terms to describe the re-radiation from the other three. This means that the analysis takes account of the zero order mutual effects only, as in Section 6.3; the higher order re-radiation is described by simple superposition as in Section 6.2.

P_0 and Q_0 are given by equation (6.17) and P_n, Q_n, for $n \neq 0$ by P_n from equation (6.5) with d replaced by $d+a$ and $d-a$ respectively. The result is written in the form:

$$g(\phi) = \left| \tilde{g}_1(\phi) + \tilde{g}_0(\phi) - f \right| \qquad (6.26)$$

in which $\tilde{g}_1(\phi)$ is the normalized re-radiation coefficient in complex form neglecting mutual effects from equation (6.13) $\tilde{g}_0(\phi)$ is the zero order complex normalized re-radiation coefficient including mutual effects from equation (6.22) and f is a factor correcting the fact that the zero order terms in $\tilde{g}_1(\phi)$ are also included in $\tilde{g}_0(\phi)$.

The result of equation (6.26) applies to systems in which βr is not necessarily small but a/r is still large enough to permit the use of zero order mutual terms only.

ALG

Printed by BBC Research Department, Kingswood Warren, Tadworth, Surrey